CHALMERS
UNIVERSITY OF TECHNOLOGY

SAFER HBM Model Development for Enhanced Submarining Prediction

Report 2024:03, Version 1.0

Main Author

Erik Brynskog

Reviewer(s) of report

Johan Iraeus, Bengt Pipkorn, Johan Davidsson

Funding

This study was funded by Strategic Vehicle Research and Innovation (FFI) (Award number: 2018-04998), by VINNOVA, the Swedish Transport Administration, Swedish Energy Agency, and industrial partners. Partners in the research project are Autoliv, Volvo Cars and Sahlgrenska University Hospital, Gothenburg, Sweden. This work has been carried out in association with SAFER – Vehicle and Traffic Safety Centre at Chalmers, Gothenburg, Sweden. The simulations were enabled by resources provided by the National Academic Infrastructure for Supercomputing in Sweden (NAISS) at Chalmers Centre for Computational Science and Engineering (C3SE) and at Linköping University National Supercomputer Centre (NSC), partially funded by the Swedish Research Council through grant agreement no. 2022/5-513 and 5-509.

DEPARTMENT OF MECHANICS AND MARITIME SCIENCES
CHALMERS UNIVERSITY OF TECHNOLOGY

REPORT 2024:03
Gothenburg, Sweden, May 2024
www.chalmers.se

Contents

1. Introduction

Submarining, defined as *"the lap belt slides over iliac crest with lap belt forces effecting the internal abdominal organs during forward displacement of the lower torso"* (Adomeit & Heger, 1975), can lead to injuries related to belt-to-abdominal loading in frontal automotive crashes. Injuries to the abdominal organs are therefore often used as a proxy for the submarining event, when studying the epidemiology of submarining scenarios from real-world data (Couturier et al., 2007; Poplin et al., 2015). Injuries to the abdominal organs can, however, stem from multiple sources, not strictly related to the submarining outcome (Poplin et al., 2015). As a result, retrospective studies of submarining in real-world crashes are difficult and a prospective approach using models is considered an important complement.

Prospective models can be both physical, *i.e.* Anthropometric Testing Devices (ATDs), or virtual, *e.g.* finite element ATDs (FE-ATDs) or FE human body models (FE-HBMs). The SAFER HBM (Pipkorn et al., 2021) is an example of an FE-HBM capable of predicting kinematics and kinetics from omnidirectional loads in varying crash scenarios. Furthermore, it can be used to study the effect of population variability by morphing based on sex, age, stature, and weight. However, the model is currently not developed/validated with the main target of submarining prediction. Limitations include, *e.g.*, orientation of the pelvis and alignment with the surrounding soft tissue that does not match the average measurements that are available in current literature, a soft tissue mesh that is unconnected to the skeleton, and elements of poor quality around the hip-thigh junction.

The aims of this report are, hence, to update and enhance the SAFER HBM v10 (Pipkorn et al., 2021) for future submarining studies in frontal automotive crashes including population variability.

2. Method

The starting point for this report was the SAFER HBM v10 (Pipkorn et al., 2021). To improve the submarining prediction capability of the model, the overall biofidelity, and prepare it for future mesh morphing studies to include population variance, several updates were made to the hip region and lower extremities of the model as outlined below.

2.1. Skeletal updates

The model was updated with a newly developed lumbar spine (Iraeus et al., 2023) and pelvis model (Brynskog et al., 2021, 2022). The pelvic angle was set to a reported average of 45° (Izumiyama et al., 2018), defined as the angle between a line that connects the superior margin of the pubic symphysis (PS) with the anterior superior iliac spine (ASIS) relative to the vertical axis in the midsagittal plane, for a vehicle occupant seated with a 24° seatback angle. The new (slightly taller) lumbar spine and the updated pelvis orientation moved the H-point inferior (24 mm) and posterior (13 mm) relative to the SAFER HBM v10. To match the new position of the hip, the legs were translated until the femur head matched the new acetabulum position without

changing the femur shape, angle, or length. The change in H-point position means that the torso length of the model has increased, this results in the vertical position of the head being slightly higher when the model is seated, compared to SAFER HBM v10.

2.2. Soft tissue updates

The target surface for the new geometry of the skin, covering the hip and thighs of the SAFER HBM, was based on the HumanShape™ (www.humanshape.org) data (Park et al., 2021), downloaded on 22 August 2022. An outer contour of a target male subject was collected in a seated posture with anthropometric variables set to the baseline for the SAFER HBM (age = 45 years, stature = 1750 mm, weight = 77 kg (Body Mass Index (BMI) = 25 kg/m^2), and a sitting height to stature (SHS) ratio = 0.52). The surface was then aligned by matching the human shape H-point with the new H-point of the model. However, several updates were required before this surface could be used as the target skin geometry of the updated SAFER HBM, motivation can be found in the Discussion.

- Firstly, there is a small difference in leg position between the HumanShape™ and the SAFER HBM. This was solved using direct morphing in ANSA v22.1.5 (Beta CAE Systems) by rotating the HumanShape™ leg around the H-point until its knee position matched that of the SAFER HBM.
- Secondly, the scans for HumanShape™ were generated from subjects seated on a rigid flat surface (Park et al., 2021), meaning that the shape of the buttocks was flatter and wider compared to an unloaded subject. An unloaded soft tissue thickness of 35-45 mm under the ischial tuberosities (Linder-Ganz et al., 2007; Wang et al., 2021), and a lateral thickness at the greater trochanter of 24 mm (Tanaka et al., 2021), was used as target measurements. To achieve these targets, 3D morph boxes were implemented in ANSA to generate a rounded geometry passing through these targets.
- Thirdly, the skin surface spanning from the abdomen to the thigh was smoothed in the HumanShape™ mesh fitting algorithm, which meant that the soft tissue thickness over the ASIS was overpredicted. Since the soft tissue thickness over the ASIS is highly dependent on the measurement direction, a 25 mm thickness, as defined in (Tanaka et al., 2021), and a 15 mm thickness, as defined in (Robinson et al., 2022), were used as target measurements and was achieved using 3D morph boxes in ANSA.

Fig. 1 a) shows the original HumanShape™ surface (light gray) versus the updated morphed version (yellow). The morphed version is also compared with the SAFER HBM v10 (orange) in **Fig. 1 b)**. To generate the updated SAFER HBM (blue), the morphed surface was used to build hexa blocks in ANSA for a full hexa mesh of the soft tissues surrounding the hips and thighs, see **Fig. 1 c)**. The target was a high-quality, all hexahedral, mesh to allow for extensive mesh morphing, which was achieved using pre-defined meshing requirements (Brynskog et al., 2022). The element formulation used for the solids was a fully integrated 8-point hexahedron with an assumed strain approach to avoid shear locking behavior seen in standard fully integrated elements, intended for elements with poor aspect ratios, (ELFORM = -2 in LS-DYNA (ANSYS Livermore Software Technology, California, United States)). While the elements typically have an aspect ratio below 5 in the lap belt area, the compression from belt

loading in simulated crashes may increase the elements aspect ratio and make them sensitive to shear locking at the time of submarining.

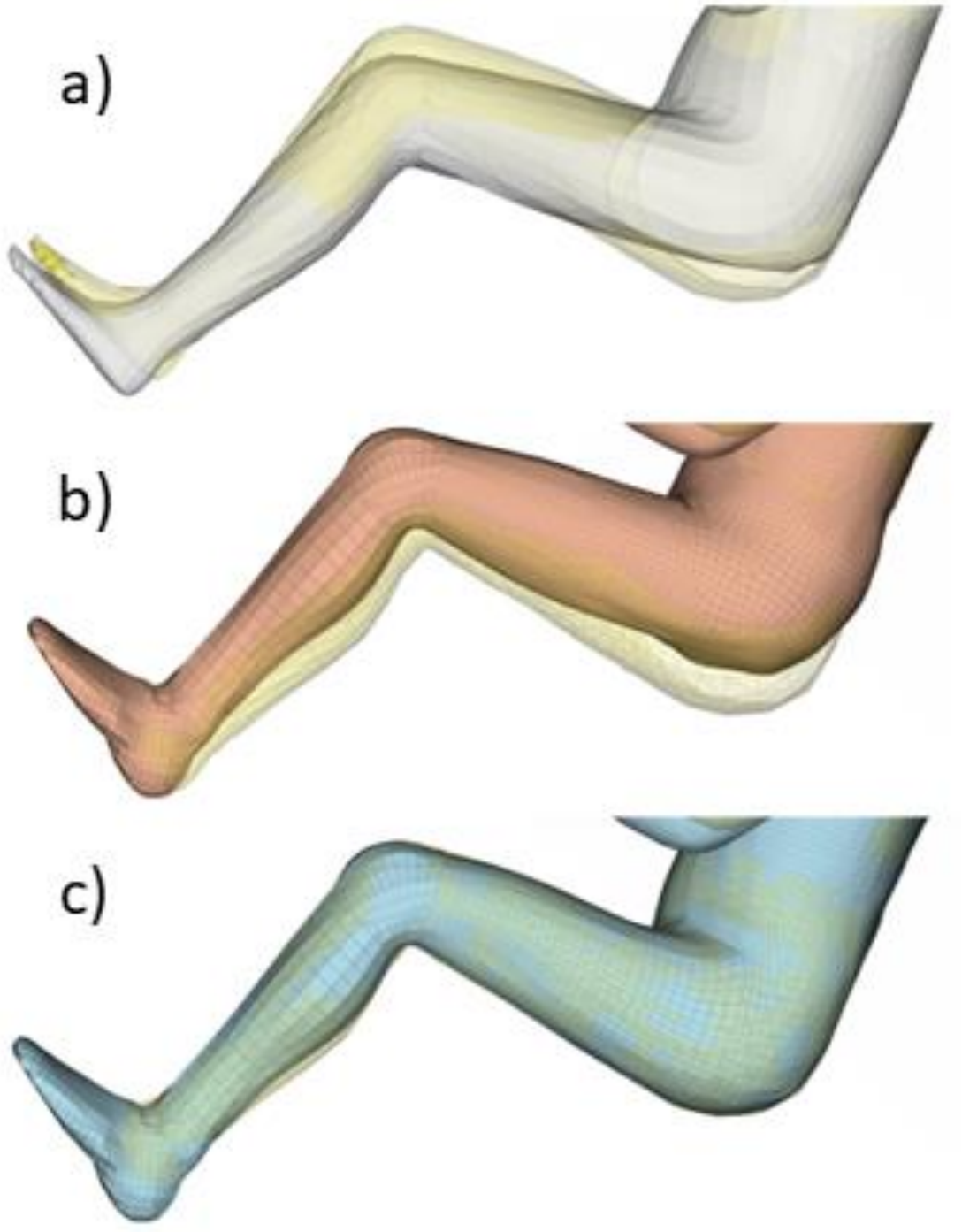

Fig. 1 Schematics of hip and thigh outer skin surfaces. The upper figure (a) shows the original HumanShape™ geometry (light gray) versus the updated morphed version (yellow), aligned at the H-point. The middle figure (b) shows the baseline model geometry, the SAFER HBM v10, (orange) versus the updated morphed geometry (yellow), aligned by the shoulder and upper torso to highlight the shorter torso length and missing buttock soft tissue. The lower figure (c) shows the updated SAFER HBM geometry (blue) versus the updated morphed geometry (yellow), aligned by the H-point (this version also matches the locations of the acromion (shoulder)).

To have a computationally efficient model that fulfills simulation efficiency requirements, the SAFER HBM does not target models of individual 3-D muscles. Instead, fat and muscle material properties were separately assigned to volumes of the soft tissue mesh that approximates the fat/muscle distribution, defined based on anatomical textbooks, see **Fig. 2**. The muscle volumes considered include the gluteal muscles, the inferior aspect of the erector spinae, and the thigh muscles. The fat material was implemented as an Ogden model using reported parameters for average fat stiffness (Naseri, 2022). However, a robust material model for passive muscle tissue, validated for compressive loading at strain rates at around 100/s, typical in simulated automotive crashes, was not found in the literature. Instead, in the search for a more suitable muscle material model, the stiff fat representation (Naseri, 2022) was evaluated against an existing muscle material model (Lanzl et al., 2021) (which was found to become unstable at strains above 40%) and was found to produce similar stress-strain results. Hence, until better muscle material models are made available, the stiff fat material properties were implemented in the updated SAFER HBM as a proxy for a passive muscle tissue material.

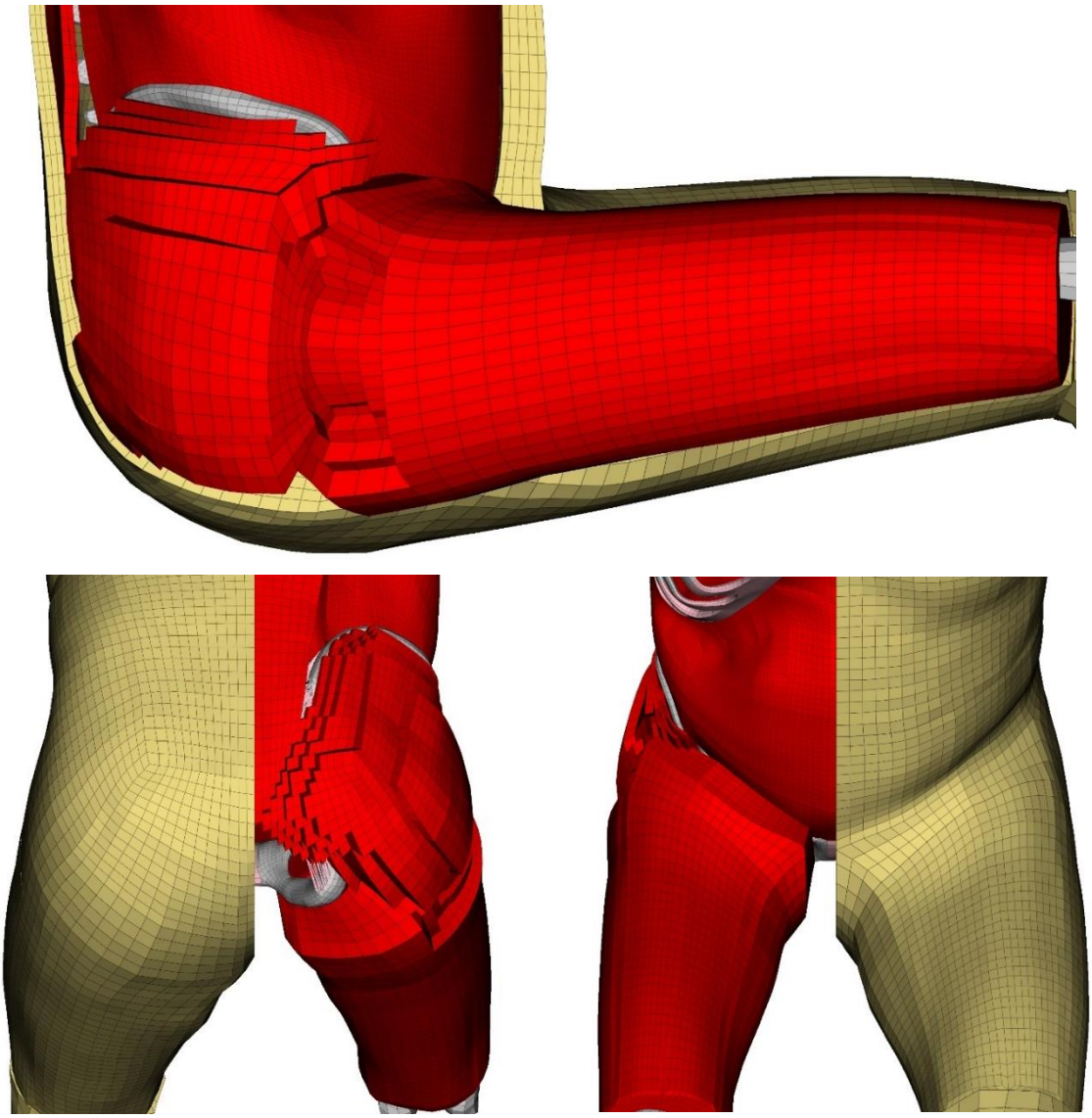

Fig. 2 Fat/muscle distribution around the thigh and buttocks. The apparent voids seen in the figure are filled with fat tissue elements.

The thigh muscle elements adjacent to the femur surface have been tied all along the femur shaft, while the elements representing the hip muscles have been connected to the pelvis model at areas approximately matching their origin/insertion. The pelvis-to-hip muscle connections were achieved by extruding a one element thick solid layer which shares nodes with the skeleton on one side and was surface aligned and tied to the muscle elements using a contact (*TIED_NODES_TO_SURFACE_OFFSET in LS-DYNA) on the other side, see **Fig. 3**. Since the function of these elements were primarily to avoid separation of the muscles from the pelvis when the muscles are pulled away from the skeleton, these solids were given material properties based on high-speed tension tests on human thigh muscles (Zhai et al., 2019). This material definition is too stiff to be used on muscle elements that mainly experience compressive loading but was considered a reasonable approximation for the simplified muscle coupling functionality.

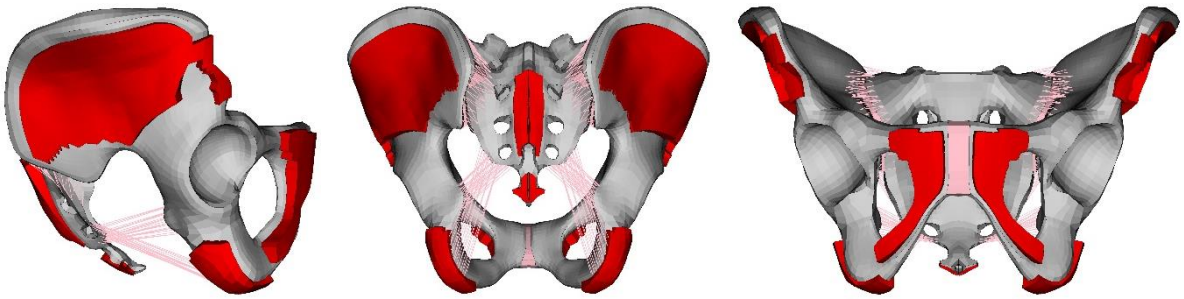

Fig. 3 Muscle attachment elements for the pelvis.

One exception to the muscle modeling strategy described above was made by the introduction of an explicitly modeled abdomen muscle wall, connecting the ribcage with the pubis rami and the iliac crest, see **Fig. 4**. The geometry for the muscle wall was created by projecting the HumanShape™ skin surface using subcutaneous adipose tissue (SAT) thickness data (Holcombe & Wang, 2014) and targeting an average male rectus abdominus muscle thickness of ~10 mm and a lateral abdominal thickness of ~18 mm (Tahan et al., 2016). A full hexa/quad mesh was then generated using HEXA BLOCKS in ANSA. The solid elements were modelled as constant stress solids (ELFORM = 1 in LS-DYNA) with a stiffness based hourglass control utilizing exact volume integration (HIQ = 5 in LS-DYNA).

A no-separation sliding-only contact (*AUTOMATIC_SURFACE_TO_SURFACE_TIEBREAK with OPTION = 4 in LS-DYNA) was modeled between the abdomen muscle wall and the abdomen subcutaneous fat on one side, and between the abdomen muscle wall and the abdominal cavity volumes, on the other side. This was implemented to replicate a fascia, connecting the muscle and fat but allowing relative movement.

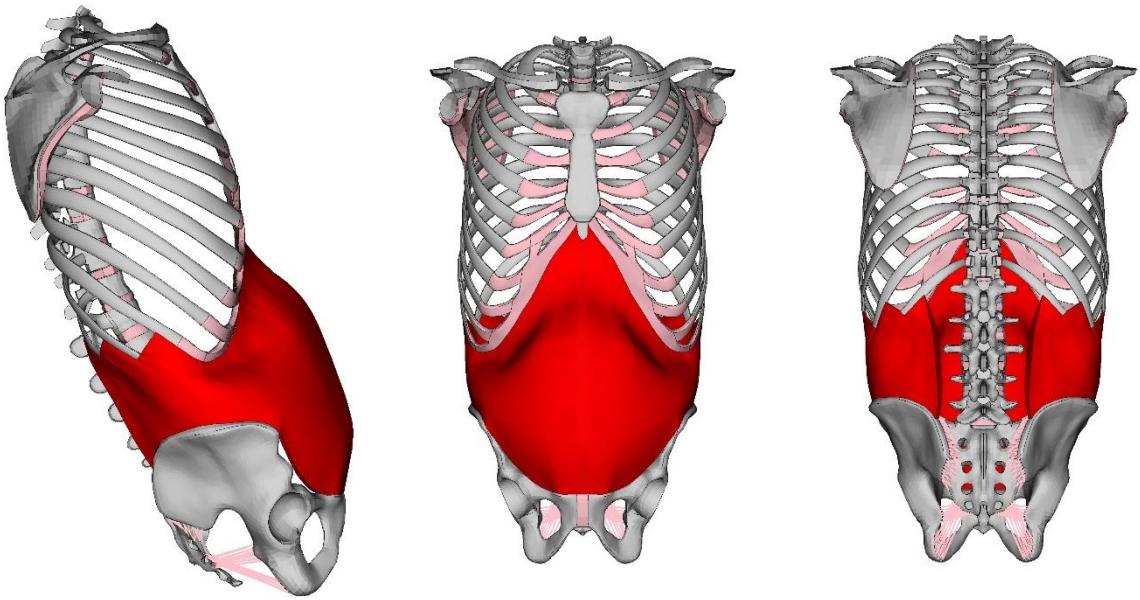

Fig. 4 New abdomen muscle wall (red) connecting the pelvis and the ribcage.

To fill the new abdomen/pelvic cavity, and improve the overall mesh quality, the lower abdomen and pelvic cavity volumes were re-meshed, see **Fig. 5**. To couple the meshed volumes with each other and the models of the surrounding skeleton, the no-separation sliding-only contact was also implemented between the lower abdomen and pelvic volumes as well as between the lower abdomen volume and parts of the spine.

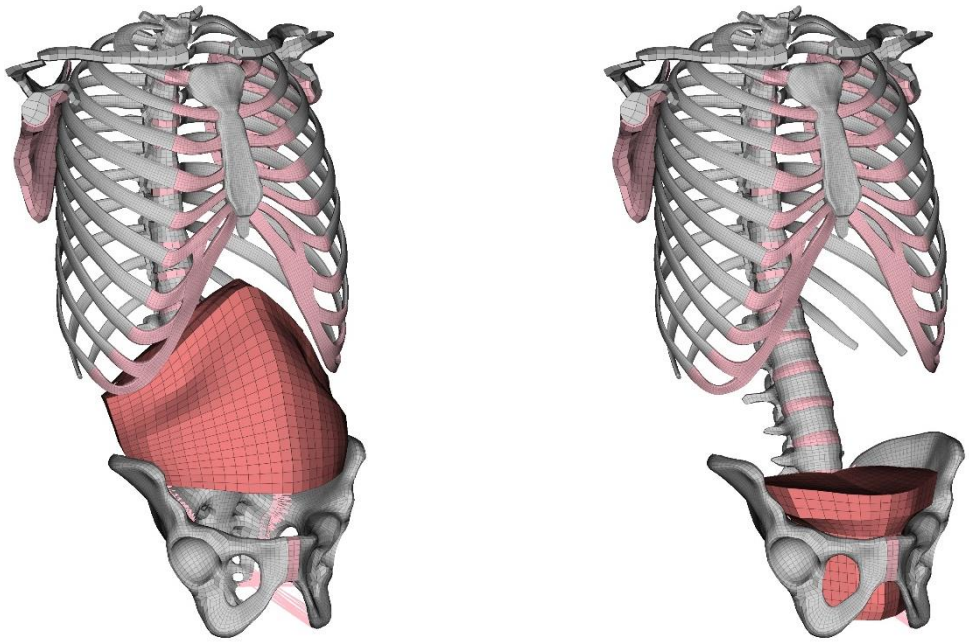

Fig. 5 Re-meshed lower abdominal cavity volume (left) and pelvic cavity volume (right).

Finally, to close the inferior opening of the bony pelvis model, the pelvic floor was modelled using fully integrated shell elements (ELFORM = 16 in LS-DYNA), where the shells bridge the pubis, ischial spine, coccyx, and sacrum, see **Fig. 6**. Since the pelvic floor acts as a support for the pelvic organs, the shells were tied (*TIED_NODES_TO_SURFACE_OFFSET in LS-DYNA) to the bottom nodes of the pelvic cavity volume. The average thickness of puborectalis and iliococcygeus has been

estimated at 5.9 mm in men (Stansfield et al., 2022) and was used for all pelvic floor elements. Since the Ogden material model was sometimes found unstable when applied to fully integrated shells, an elastic stiffness of 1 MPa was estimated from the tension tests by (Zhai et al., 2019) and implemented using *MAT_ELASTIC.

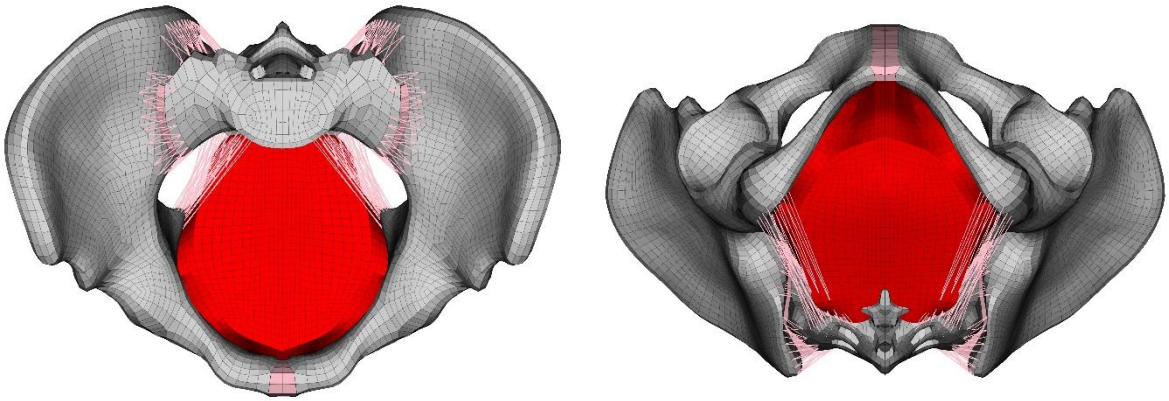

Fig. 6 Shell representation of pelvic floor muscle from superior view (left) and inferior view (right).

2.3. Joint updates

The hip, knee, and ankle joints of the SAFER HBM v10 was found to be stiffer than data in appropriate literature (Amankwah et al., 2004; Riener & Edrich, 1999), especially the ankle joint which was ~10x stiffer. The stiffness of these joints will affect the force going through the legs, which will influence the pelvis kinematics, in a frontal impact. Correct pelvis kinematics had the highest priority for this update since the aim was to enhance the models submarining prediction capability. Hence, it was decided to remove the ligaments and tendons of the hip, knee, and ankle joint, and instead use the kinematic joints already implemented for the active version of the SAFER HBM (Östh et al., 2014). In addition, since the material of the skin and soft tissues in the lower leg and foot were found to significantly add stiffness to the joints they were replaced with softer versions, already implemented in the torso and neck (Pipkorn et al., 2021). The flexion/extension stiffness of each joint were prescribed using passive joint moments and compared with results predicted for volunteer (Riener & Edrich, 1999) when computed using the SAFER HBM modelled joint angles (ankle = 4°, knee = 67°, hip = 88°), see **Fig. 7**. The initial peak (around the zero rotation) seen in the simulated response of knee and hip rotation comes from the inertia of the moving limb, since the rotation was applied as a constant velocity with a ramp of 50 ms.

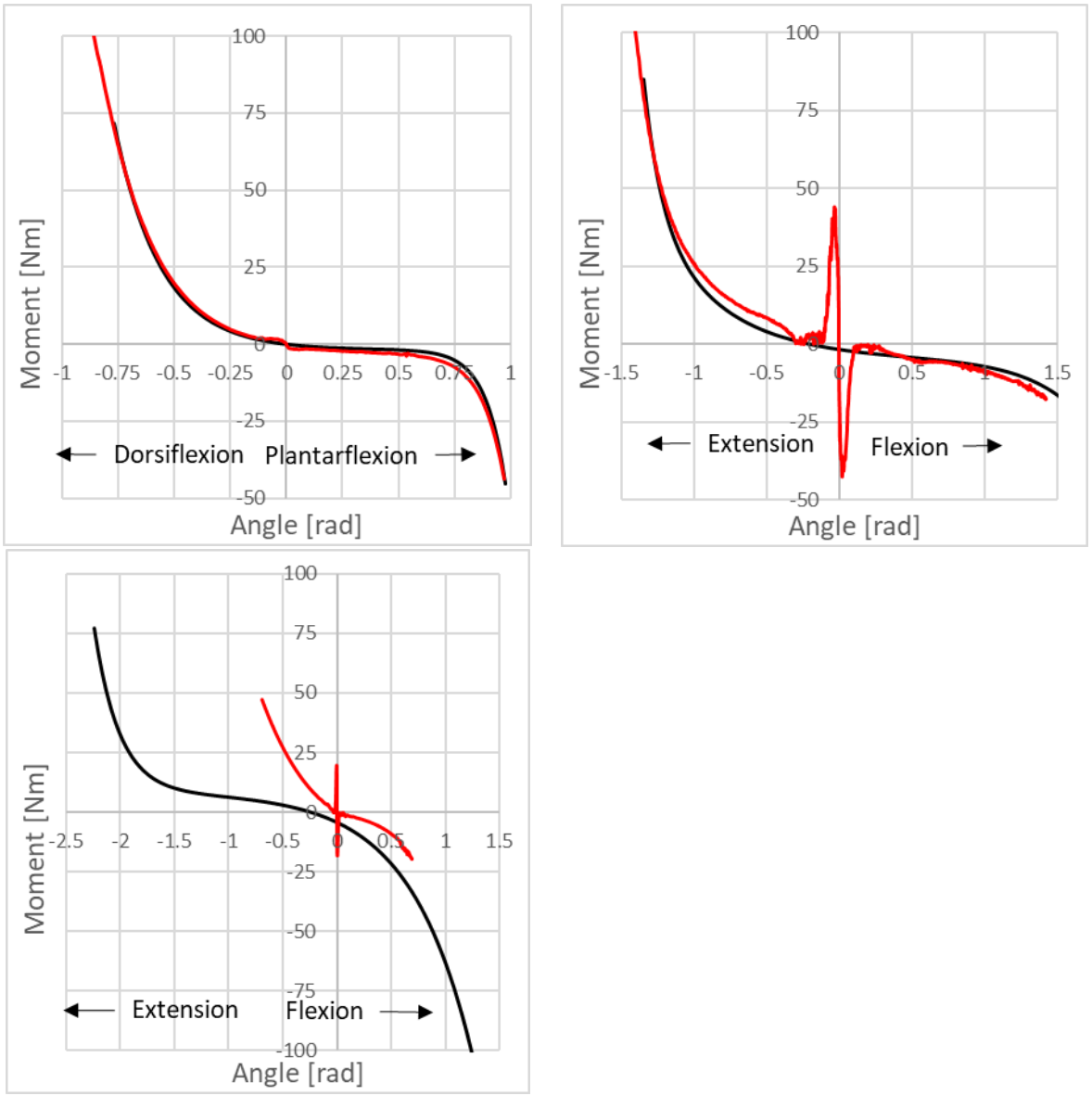

Fig. 7 Passive joint moments for ankle (top left), knee (top right), and hip (bottom left) from volunteers (black) based on the SAFER HBM modelled joint angles (ankle = 4°, knee = 67°, hip = 88°) vs. updated kinematic joints (red). The curves are offset such that 0 rad corresponds to the SAFER HBM modelled joint angle of each joint. The initial peak (around the zero rotation) seen in the simulated response of knee and hip rotation comes from the inertia of the moving limb, since the rotation was applied as a constant velocity with a ramp of 50 ms.

2.4. Simulations

To check the feasibility of the model updates, four simulation scenarios were analyzed. These include gravity settling on a rigid plate to assess soft tissue deformation, free-back rigid bar impacts to the abdomen (Hardy et al., 2001), quasi-static whole body lumbar flexion (Uriot et al., 2015b), and semi-rigid seat sled tests resulting in both submarining and no submarining outcomes (Uriot et al., 2015a). All simulations were

performed using LS-DYNA MPP R12.2.1 (ANSYS Livermore Software Technology, California, United States) on a cluster running with 32 cores.

Gravity settling

The gravity settling simulation was performed from an upright posture on a rigid plate. Gravity was applied from the start of the simulation while constraining the model in the sagittal plane. Wrists and ankles were also constrained in the vertical direction to avoid free falling limbs affecting the response. A critical damping value, defined to remove model oscillations, was applied for the first 250 ms and was linearly removed between 250 and 300 ms. At 300 ms the deformation of the soft tissue inferior to the ischial tuberosities and lateral to the greater trochanter was evaluated.

Free-back rigid bar abdominal impacts (Hardy et al., 2001)

The model was placed in an upright posture on a rigid plate with gravity settling applied for the first 300 ms, as in the gravity settling evaluation. At 300 ms, the model was completely released from all constraints as a rigid bar (25 mm in diameter with a weight of 48 kg) impacted the model at the umbilical/L3 level at a low (6.3 m/s) and high (9.2 m/s) impact seed.

Whole body lumbar flexion (Uriot et al., 2015b)

The model was placed in a rigid seat with 90° between seat and backrest. A lap belt was used to couple the model with the rigid seat applying a belt load of 100 N to each side during the first 200 ms. To mimic the back-plate and chest belt, used in the experiment to couple the PMHS torso with the rotating frame, the spine was made rigid from T10 to head and constrained as one part to T7. The T7 vertebrae was then constrained to a rigid plate aligned with the superior endplate of sacrum, defined as the rotation center of the frame. At 200 ms, the rigid plate was rotated at 20°/s until reaching a lumbar flexion of 30°.

Sled test with semi-rigid seat (Uriot et al., 2015a)

A sled test with a semi-rigid seat aimed to replicate a front (non-submarining) setup and a rear (submarining) setup was simulated. The setup used a 2-point shoulder and a 2-point lap belt with separate load limiters and applied an acceleration pulse with an approximate peak of 300 m/s^2 (-14 m/s final sled velocity). The belt was modeled 45 mm wide and 1.2 mm thick with a belt stretch of 9% at a tension of 10 kN. The mesh consisted of 6 elements across the width of the belt and a coated 2D seatbelt material (*MAT_B01_2D in LS-DYNA) for added bending stiffness (Soni et al., 2021). The belt to HBM friction coefficient was set at 0.25 while the seat to HBM friction coefficient was set at 0.2. A belt pre-load of 50 N was applied to each retractor based on input from the study authors. The belt payout was used as a calibration variable to match the recorded belt force initiation. Following gravity settling, as in the gravity settling evaluation, the recorded acceleration pulse was applied to the rigid seat with no additional constraints on the HBM. Differences between the front and rear seat configuration include modified seat positions, belt anchor point positions, and seat stiffness, as described in the experiment reference.

3. Results

The new hip and thigh mesh of the soft tissues consists of 40,724 solids and 10,160 shells, with an average element length of 5 mm, compared to the old model which had 32,184 solids and 8,460 shells and an average element length of 6 mm. In addition, the new abdomen wall mesh consists of 13,424 solids and 13,512 shells, with an average element length of 3 mm. The quality of all elements was within the 100% limits as specified in (Brynskog et al., 2022).

Gravity settling

In the gravity settling simulation, the soft tissue under the ischial tuberosities compressed by 20 mm, compared to in-vivo measurements for an average male ranging between 13-35 mm (Linder-Ganz et al., 2007; Wang et al., 2021), while flowing laterally to the greater trochanter by 9 mm, compared to standing to seated in-vivo measurements for an average male, reported at 13 mm (Tanaka et al., 2021), see **Fig. 8**.

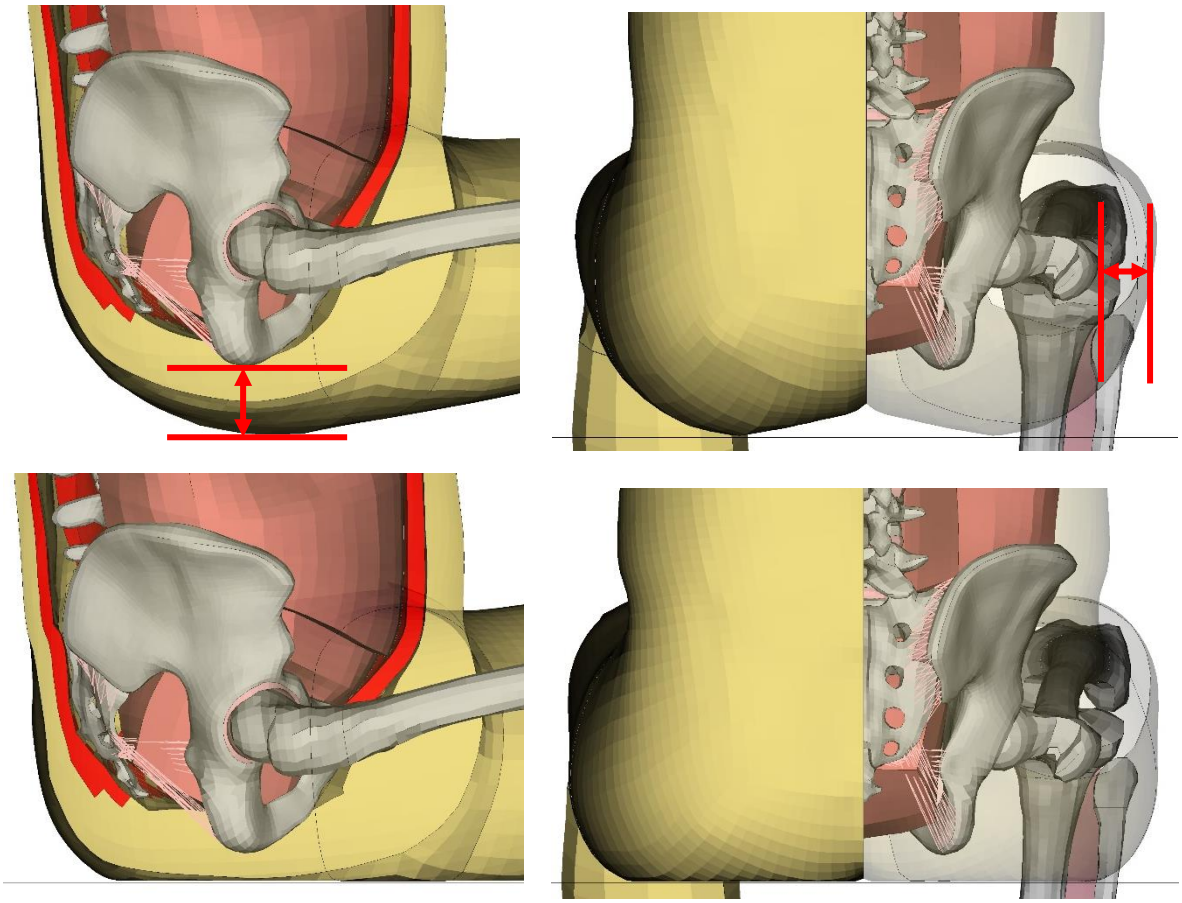

Fig. 8 Uncompressed soft tissue (top row) and gravity compressed soft tissue (bottom row). Red arrows indicate measurements taken for inferior (top left) and lateral (top right) soft tissue deformation.

Free-back rigid-bar abdominal impacts (Hardy et al., 2001)

In the rigid-bar impact simulations, the model response stayed mostly within the PMHS corridor, see **Fig. 9**. In the low-speed impact the bar goes in contact with the lumbar spine at the peak penetration of ~150 mm. Hence, the penetration found in the experiments of 170-210 mm can only be achieved by a more protruding abdomen (greater abdominal penetration before lumbar spine contact). In the high-speed impact the bar again stops at roughly the same amount of abdominal penetration but this time it matches better with the peak average PMHS penetration. This indicates that the abdomen shape for the SAFER HBM was more like those of the PMHSs in the high-speed experiments.

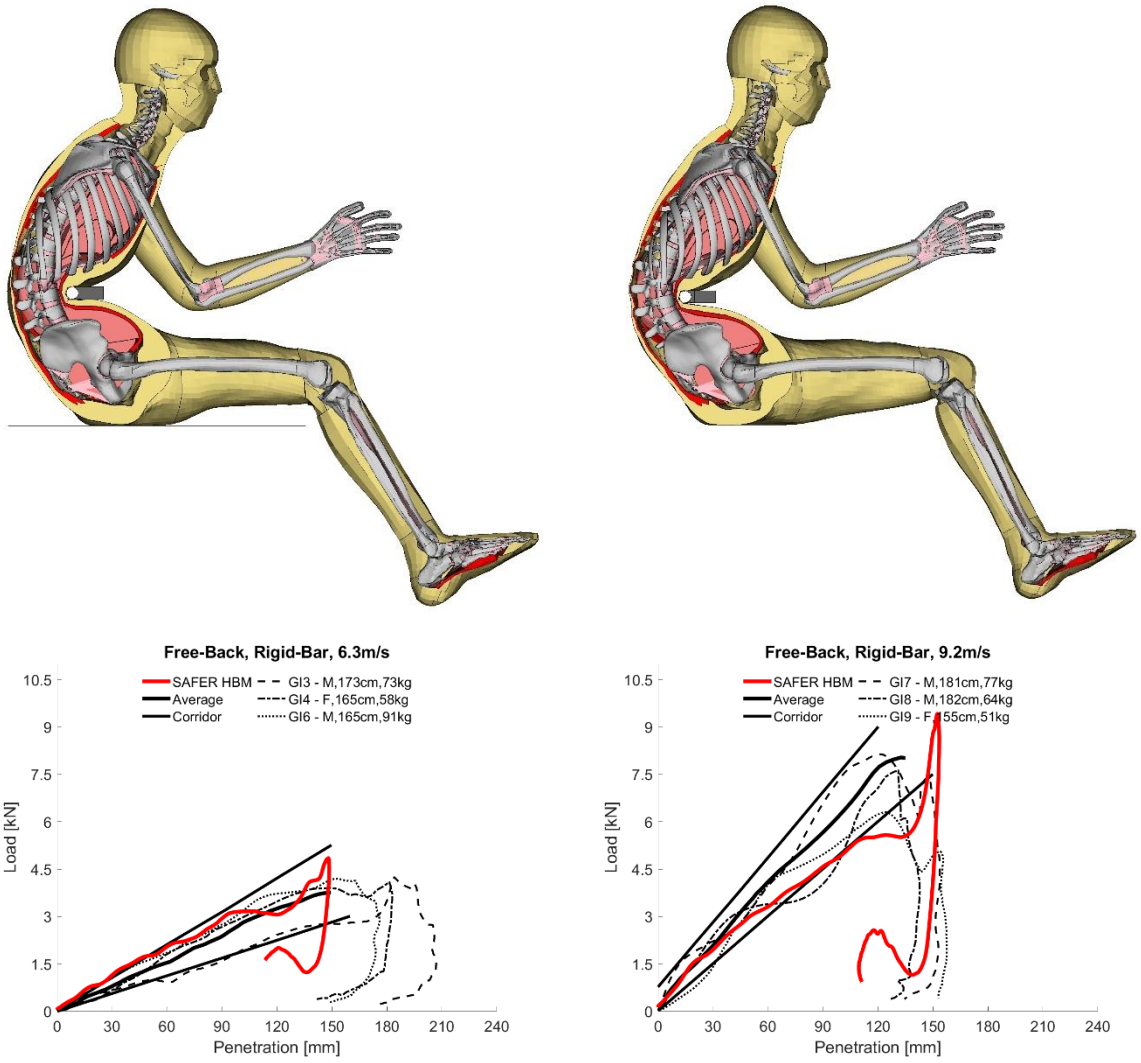

Fig. 9 Free-back rigid-bar impacts at low (6.3 m/s) (left) and high (9.2 m/s) (right) impact speeds comparing the response of the updated SAFER HBM (red) with PMHSs (black).

Whole body lumbar flexion (Uriot et al., 2015b)

In the lumbar flexion simulations, the model response followed the average PMHS response, except for an initial moment peak due to inertia of the torso since the rotation was applied at a constant velocity with a ramp of 50 ms, see **Fig. 10**. The experiment was performed quasi-static, however, that is not feasible using an explicit FE model due to time limitations. Instead, the target flexion was reached in about 2 s of simulation time at the expense of some initial inertia effects. Applying the load slower and with a smoother ramp would lower the initial peak/oscillation but does not substantially change the later part of the curve.

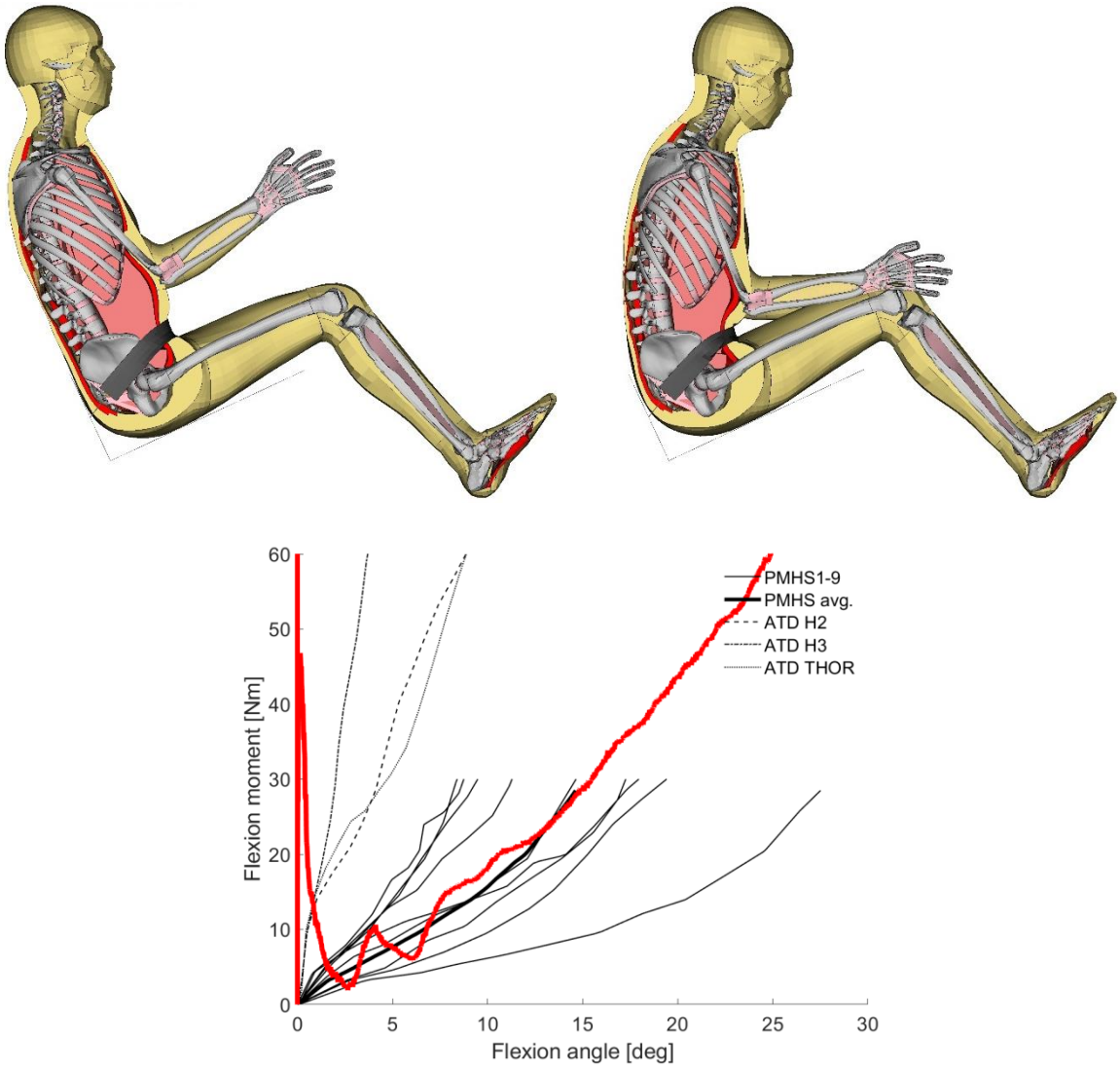

Fig. 10 Initial position (top left) and position at 25° torso flexion (top right) with flexion moment vs. flexion angle (bottom) comparing the response of the updated SAFER HBM (red) with PMHSs (black).

Sled test with semi-rigid seat (Uriot et al., 2015a)

In the sled simulations, the model correctly predicted no submarining for the front seat configuration and submarining for the rear seat configuration, see **Fig. 11**. The model response also stayed mostly within the PMHS envelopes for both the boundary condition and the kinematic signals in both configurations, see **Fig. 12** to **Fig. 15**. The main differences when comparing the results were a slight over-rotation for the pelvis at the time of submarining and a more pronounced lap belt force drop following submarining, both in the rear seat configuration.

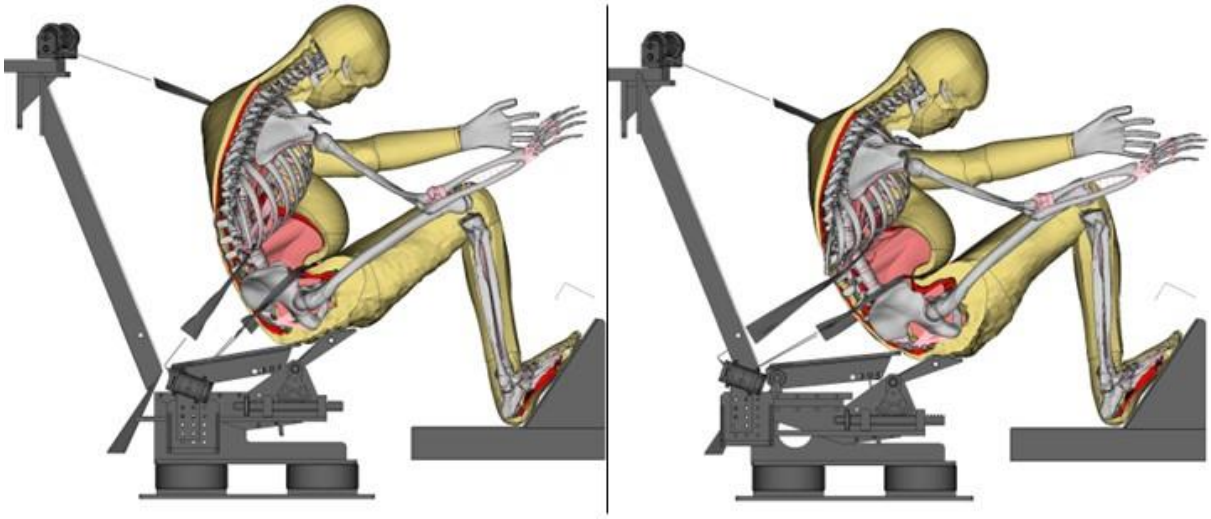

Fig. 11 A non-submarining front seat response (left) and a submarining rear seat response (right).

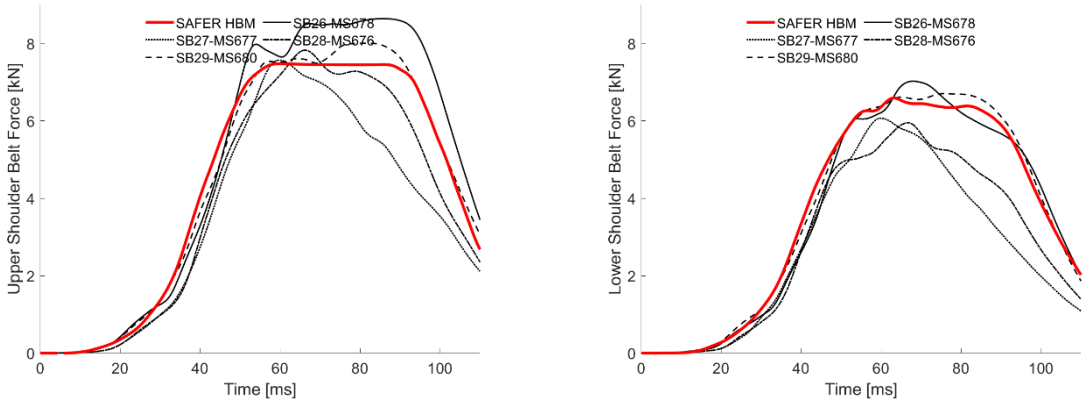

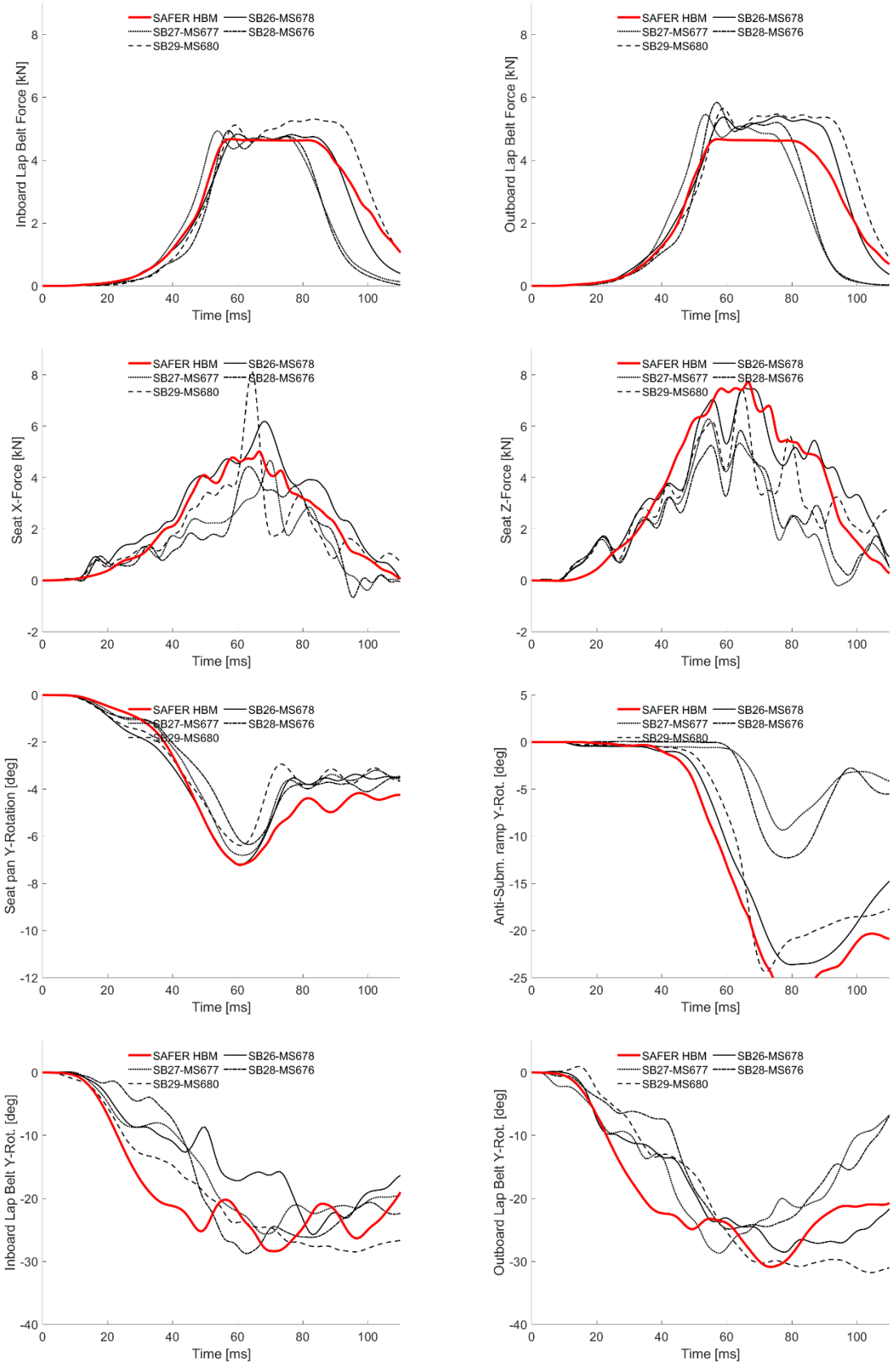

Fig. 12 Boundary condition signals for SAFER HBM (red) compared to PMHS response (black) in the front seat configuration.

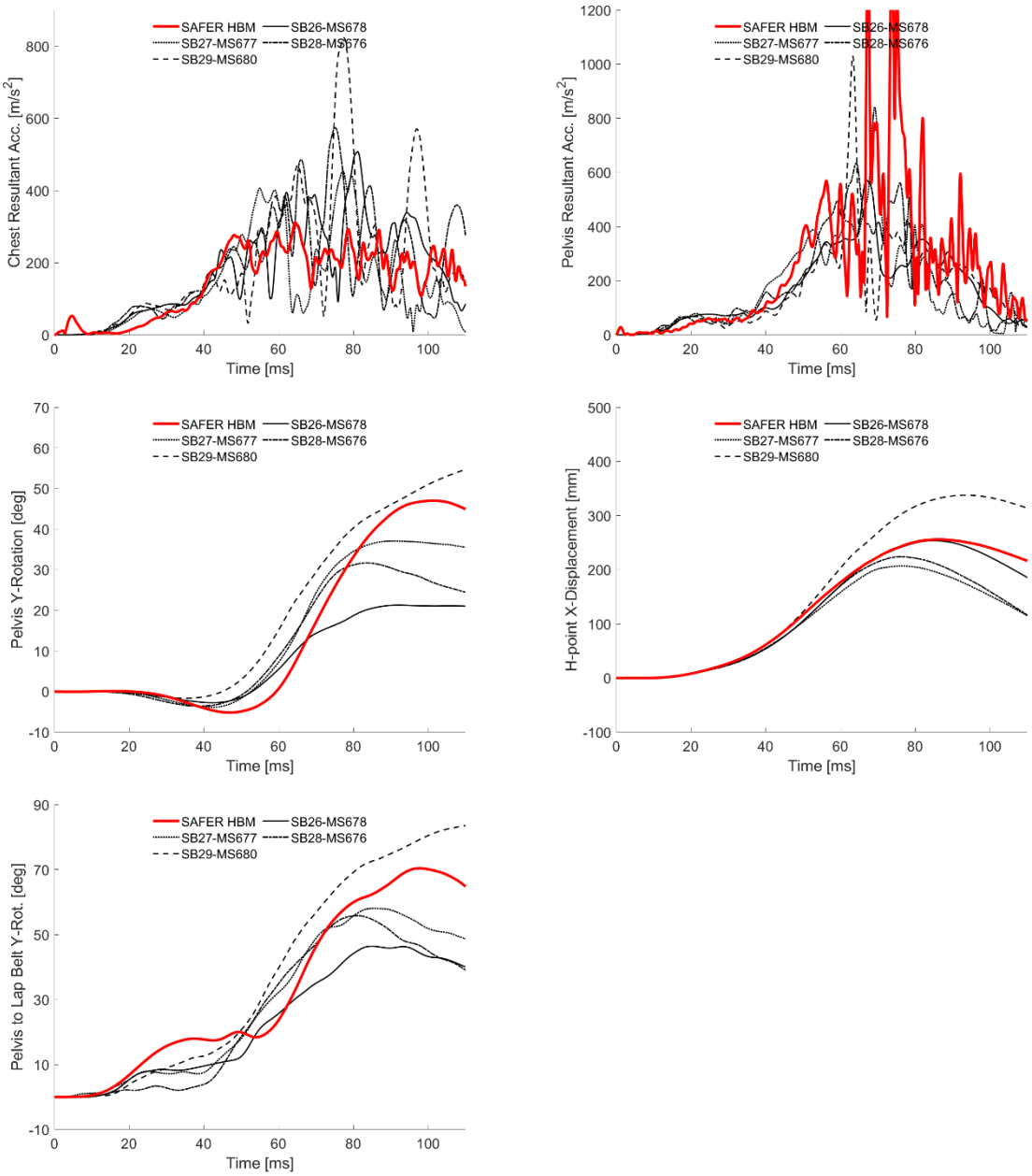

Fig. 13 Kinematic signals for SAFER HBM (red) compared to PMHS response (black) in the front seat configuration.

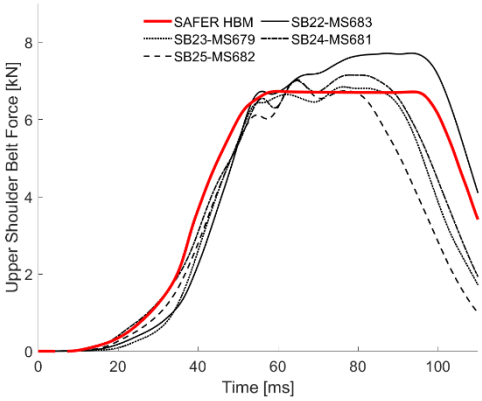
SAFER HBM
SB22-MS683
SB23-MS679
SB24-MS681
SB25-MS682
Upper Shoulder Belt Force [kN]
Time [ms]

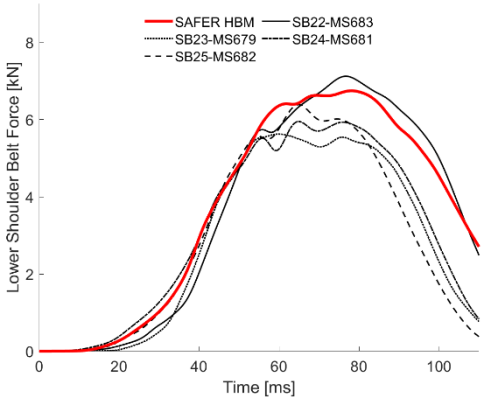
SAFER HBM
SB22-MS683
SB23-MS679
SB24-MS681
SB25-MS682
Lower Shoulder Belt Force [kN]
Time [ms]

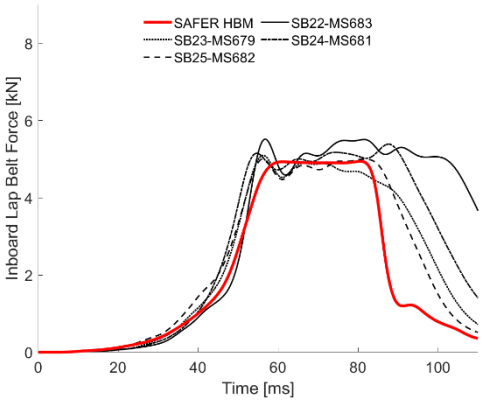
SAFER HBM
SB22-MS683
SB23-MS679
SB24-MS681
SB25-MS682
Inboard Lap Belt Force [kN]
Time [ms]

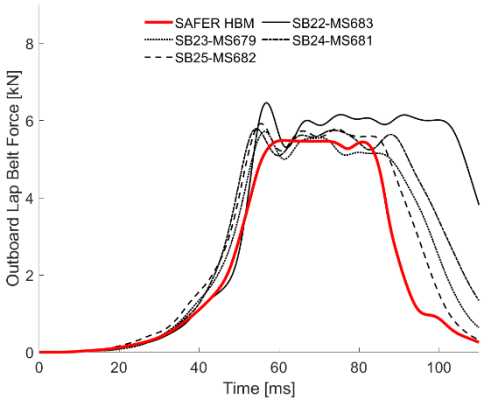
SAFER HBM
SB22-MS683
SB23-MS679
SB24-MS681
SB25-MS682
Outboard Lap Belt Force [kN]
Time [ms]

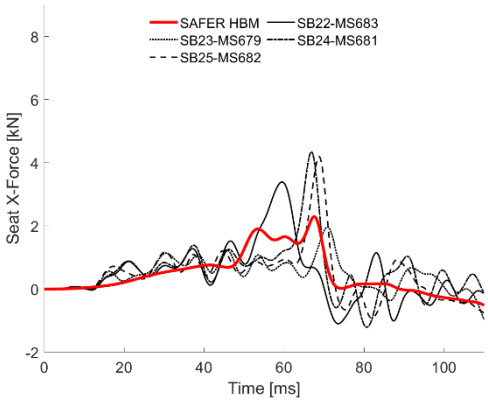
SAFER HBM
SB22-MS683
SB23-MS679
SB24-MS681
SB25-MS682
Seat X-Force [kN]
Time [ms]

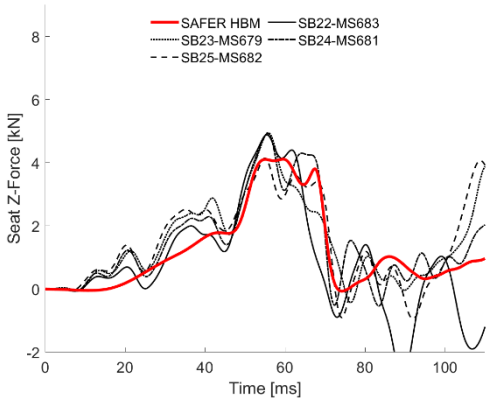
SAFER HBM
SB22-MS683
SB23-MS679
SB24-MS681
SB25-MS682
Seat Z-Force [kN]
Time [ms]

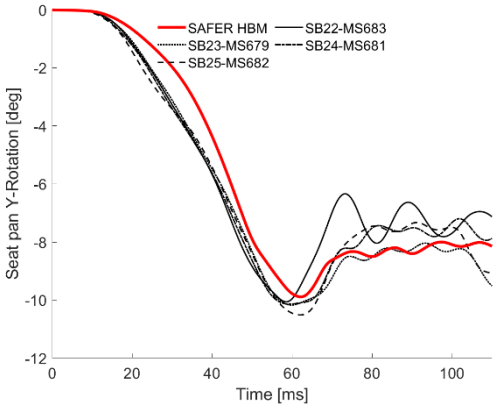
SAFER HBM
SB22-MS683
SB23-MS679
SB24-MS681
SB25-MS682
Seat pan Y-Rotation [deg]
Time [ms]

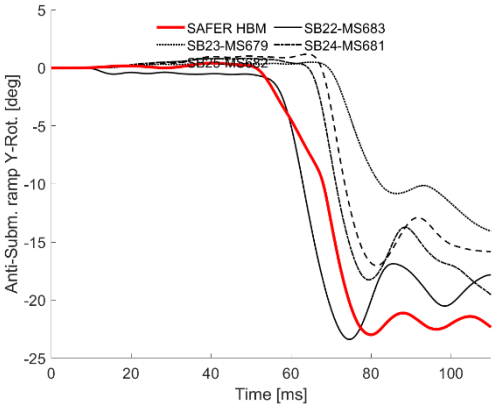
SAFER HBM
SB22-MS683
SB23-MS679
SB24-MS681
Anti-Subm. ramp Y-Rot. [deg]
Time [ms]

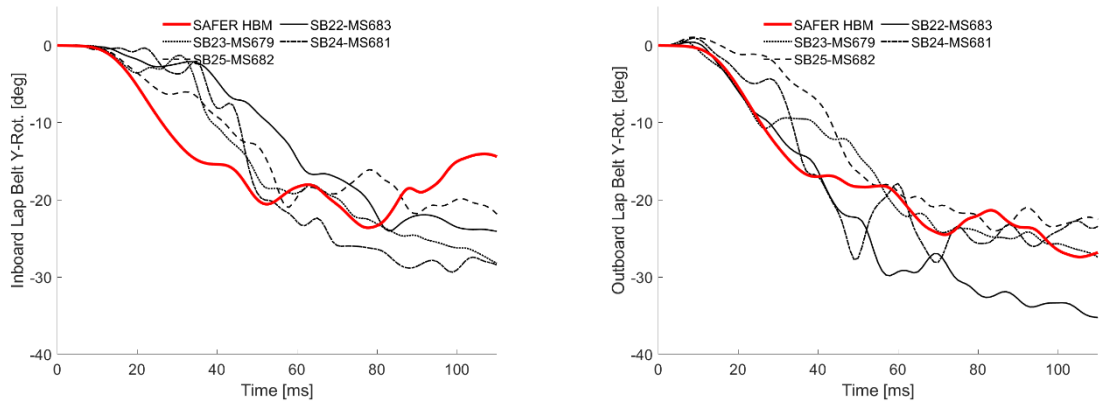

Fig. 14 Boundary condition signals for SAFER HBM (red) compared to PMHS response (black) in the rear seat configuration.

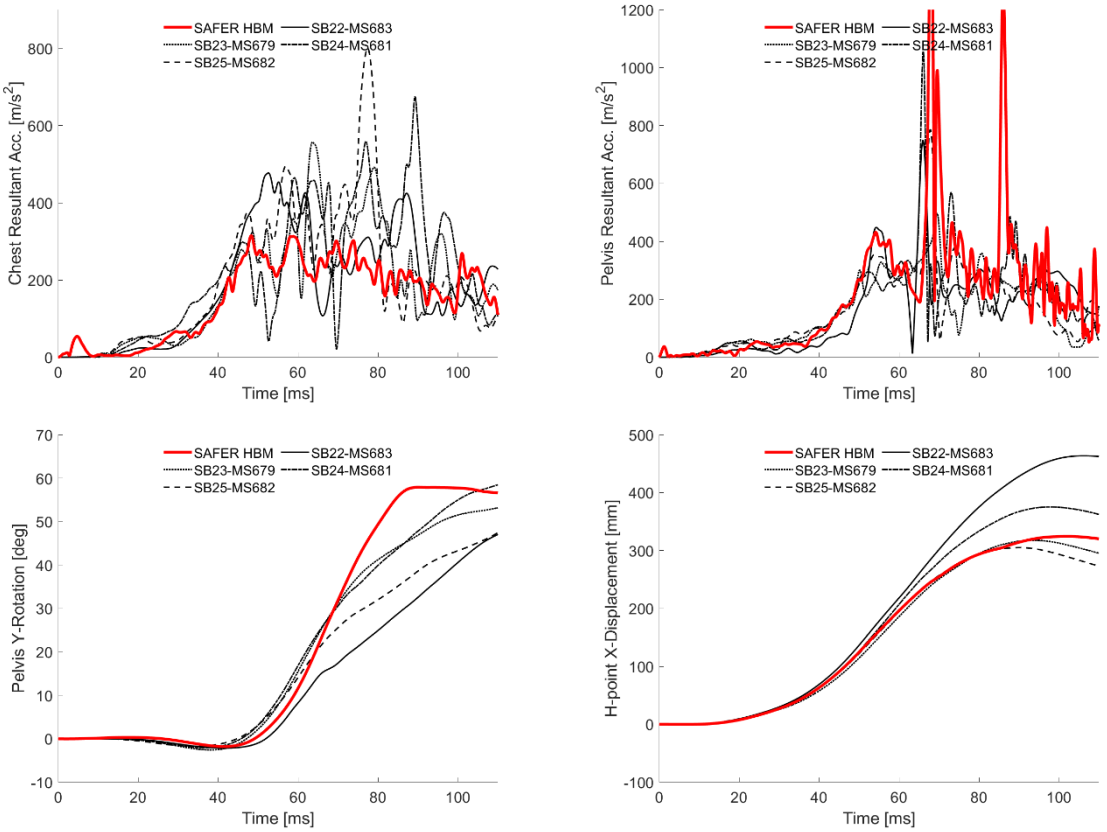

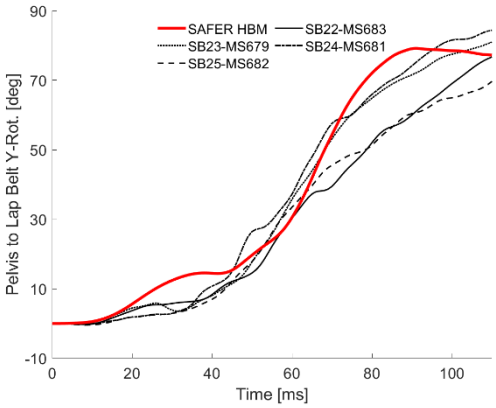

Fig. 15 Kinematic signals for SAFER HBM (red) compared to PMHS response (black) in the rear seat configuration.

4. Discussion

The scans for HumanShape™ were generated from subjects seated on a rigid flat surface (Park et al., 2021), meaning that the shape of the buttocks was flatter than if the subjects would have been unloaded. An unloaded soft tissue thickness of 35-45 mm under the ischial tuberosities has been reported (Linder-Ganz et al., 2007; Wang et al., 2021). Furthermore, since the soft tissue is close to incompressible it flows laterally when compressed, making the HumanShape™ surface wider over the hips compared to an unloaded subject. A lateral thickness at the greater trochanter of 24 mm, for a standing (uncompressed) subject with BMI = 25 kg/m^2, has been reported (Tanaka et al., 2021). In addition, the skin surface spanning from the abdomen to the thigh was smoothed in the HumanShape™ mesh fitting algorithm, which means that the soft tissue thickness over the ASIS was overpredicted. Using the anthropometry of the SAFER HBM, a SAT thickness of 8-13 mm could be expected at the ASIS in a supine position (Holcombe & Wang, 2014), however, it is likely that this thickness increases in a seated posture. For standing, upright seated, and reclined seated subjects, a SAT thickness of approximately 20-25 mm (measured along a vector spanning from posterior superior iliac spine to ASIS projected on the sagittal plane at the ASIS) has been reported for a male with BMI = 25 kg/m^2 (Tanaka et al., 2021). A non-peer reviewed publication with a smaller sample indicates that for normal BMI in a seated posture, the SAT thickness is approximately 15 mm (measured along a vector going from the anterior corner of the sacroiliac joint to the ASIS) (Robinson et al., 2022). Since these measurements can both be true at the same time, due to the different definitions, they were both used as target measurements when generating the morphed version of the HumanShape™, used as the updated SAFER HBM skin geometry.

The interaction between abdominal fat and muscle tissue was modeled using a tiebreak contact that only allows tangential movement with frictional sliding. This sliding-only interface was chosen to replicate the quite substantial relative motion that can occur in facias, separating fat and muscle tissues. Using the GHBMC HBM, it has been shown that splitting a node-to-node tied coupling for the soft tissue in the ASIS region improved the submarining prediction of an obese model (Sun et al., 2019), however, this solution was not considered biofidelic. The simplified fascia model implemented in this update for the SAFER HBM was considered a way to release the interface constraint in the ASIS region with a biofidelic motivation. This type of interaction is already modeled for the ribcage, to allow the thorax soft tissue mesh to slide on the ribcage surface without separation (Pipkorn et al., 2021).

The resulting joint stiffness for the kinematic joints matches the volunteer data for the ankle and knee joint (Riener & Edrich, 1999), but is offset and builds stiffness too rapidly in hip extension. The difference for the hip joint indicates that the modelled leg position for the SAFER HBM (knee angle = 67°, hip angle = 88°) is not the neutral position of the leg, meaning that there should be a small build-up of torque (~4Nm) at this position. Adding this offset to the simulated response would improve the comparison for joint flexion, indicating that the slope of the moment curve for 0.5 rad (~30°) flexion is comparable. However, in extension the shape of the curve does not match the reference and the joint builds stiffness too rapidly. This is because the hip joint has a large range of “moment-free” rotation, and because the modelled position is some

angle from the neutral position. In reality, the soft tissue superior to the joint should, hence, be compressed while the soft tissue inferior to the joint should be stretched. This will cause the superior tissue to have some slack as the joint moves in extension, while the inferior tissue will produce a pulling force. As a result, the passive joint moment should remain close to zero for a substantial extension of the leg (~70-80° from the modelled position). In simulation this is not the result since the modelled position is treated as the neutral position. This means that the superior tissue begins to resist the extension movement as soon as the rotation starts, while the inferior tissue lacks any pulling force and could instead work against the extension movement as the soft tissue gets compressed. As a result, the moment required to move the hip joint is roughly 25 Nm greater for the model compared to the reference at 30° extension from the initial position.

In all simulations performed with the updated model, the response was mostly within the PMHS envelopes of the published reference data. This includes soft tissue deformation from gravity settling, abdomen stiffness from rigid bar impacts, lumbar spine stiffness from full-body flexion, and submarining / non-submarining outcomes from sled tests. All simulations resulted in normal termination. This indicates that the updated version of the SAFER HBM is a reasonable candidate for further submarining evaluations of variations in both boundary conditions and subject anthropometry.

The work presented in this report was used as a starting point when developing the SAFER HBM v11.

5. References

Adomeit, D., & Heger, A. (1975). Motion Sequence Criteria and Design Proposals for Restraint Devices in Order to Avoid Unfavorable Biomechanic Conditions and Submarining. *SAE Transactions*, *84*, 3150–3159. https://www.jstor.org/stable/44633645?seq=9

Amankwah, K., Triolo, R. J., & Kirsch, R. (2004). Effects of spinal cord injury on lower-limb passive joint moments revealed through a nonlinear viscoelastic model. *Journal of Rehabilitation Research & Development*, *41*(1), 15–32.

Brynskog, E., Iraeus, J., Pipkorn, B., & Davidsson, J. (2022). Population Variance in Pelvic Response to Lateral Impacts - A Global Sensitivity Analysis. *IRCOBI Conference*.

Brynskog, E., Iraeus, J., Reed, M. P., & Davidsson, J. (2021). Predicting pelvis geometry using a morphometric model with overall anthropometric variables. *Journal of Biomechanics*, *126*. https://doi.org/10.1016/J.JBIOMECH.2021.110633

Couturier, S., Faure, J., Satué, R., Huguet, J., & Hordonneau, J. (2007). Procedure to Assess Submarining in Frontal Impact. *20th International Technical Conference on the Enhanced Safety of Vehicles*. https://doi.org/10.1080/00222933.2011.563138

Hardy, W. N., Schneider, L. W., & Rouhana, S. W. (2001). Abdominal impact response to rigid-bar, seatbelt, and airbag loading. *Stapp Car Crash Journal*, *45*(November), 1–32. https://doi.org/10.4271/2001-22-0001

Holcombe, S. A., & Wang, S. C. (2014). Subcutaneous Fat Distribution in the Human Torso. *IRCOBI Conference*.

Iraeus, J., Poojary, Y. N., Jaber, L., John, J., & Davidsson, J. (2023). A new open-source finite element lumbar spine model, its tuning and validation, and development of a tissue-based injury risk function for compression fractures. *IRCOBI Conference*.

Izumiyama, T., Nishida, N., Iwanaga, H., Chen, X., Ohgi, J., Mori, K., Hayashi, T., Sakuramoto, I., Asahi, R., Sugimoto, S., & Ueno, M. (2018). The Analysis of an Individual Difference in Human Skeletal Alignment in Seated Posture and Occupant Behavior Using HBMs. *IRCOBI Conference*.

Lanzl, F., Berger, A., Huehn, D., Dussinger, S., Ghosh, P., Mayer, C., Martynenko, O., Naseri, H., Iraeus, J., & Peldschus, S. (2021). Simplified multi-code model for passive muscle tissue under impact. *IRCOBI Conference Short Communication*.

Linder-Ganz, E., Shabshin, N., Itzchak, Y., & Gefen, A. (2007). Assessment of mechanical conditions in sub-dermal tissues during sitting: A combined experimental-MRI and finite element approach. *Journal of Biomechanics*, *40*(7), 1443–1454. https://doi.org/10.1016/J.JBIOMECH.2006.06.020

Naseri, H. (2022). *Calibration of Adipose tissue material properties in LS-DYNA Hosein Naseri*. https://research.chalmers.se/publication/523470

Östh, J., Eliasson, E., Happee, R., & Brolin, K. (2014). A method to model anticipatory postural control in driver braking events. *Gait & Posture*, *40*(4), 664–669. https://doi.org/10.1016/J.GAITPOST.2014.07.021

Park, B. K. D., Jones, M. L. H., Ebert, S., & Reed, M. P. (2021). A parametric modeling of adult body shape in a supported seated posture including effects of age. *Ergonomics*, *65*(6), 795–803. https://doi.org/10.1080/00140139.2021.1992020

Pipkorn, B., Östh, J., Brynskog, E., Larsson, E., Rydqvist, L., Iraeus, J., Perez-Rapela, D., & Jakobsson, L. (2021). Validation of the SAFER Human Body Model Kinematics in Far-Side Impacts. *IRCOBI Conference*.

Poplin, G. S., McMurry, T. L., Forman, J. L., Hartka, T., Park, G., Shaw, G., Shin, J., Kim, H. joo, & Crandall, J. (2015). Nature and etiology of hollow-organ abdominal injuries in frontal crashes. *Accident Analysis & Prevention*, *78*, 51–57. https://doi.org/https://doi.org/10.1016/j.aap.2015.02.015

Riener, R., & Edrich, T. (1999). Identification of passive elastic joint moments in the lower extremities. *Journal of Biomechanics*, *32*(5), 539–544. https://doi.org/10.1016/S0021-9290(99)00009-3

Robinson, A. S., Efobi, S., Aira, J., Moore, A., Lenchik, L., Weaver, A. A., Hsu, F., Hallman, J., & Gayzik, F. S. (2022). Effect of Posture on Subcutaneous Adipose Tissue: A Preliminary Imaging Study. *The Ohio State University Injury Biomechanics Symposium*.

Soni, A., Schilling, S., Grikschat, M., Jagalur, S., Chandra, N., Venkatesh, S., Puttegowda, N., Vishwanatha, A., & Dahlgren, M. (2021). Parameter Identification of Coating Parameters to Improve Webbing Bending Response in Passive Safety Crash Simulations. *13th European LS-DYNA Conference*.

Stansfield, E., Mitteroecker, P., Umek, W., & Fischer, B. (2022). The variation in shape and thickness of the pelvic floor musculature in males and females: a geometric-morphometric analysis. *International Urogynecology Journal*, *1*, 1–9. https://doi.org/10.1007/S00192-022-05311-5/FIGURES/5

Sun, Z., Gepner, B., & Kerrigan, J. (2019). New Approaches in Modeling Belt-flesh-pelvis Interaction Using Obese Ghbmc Models. *ESV Conference*.

Tahan, N., Khademi-Kalantari, K., Mohseni-Bandpei, M. A., Mikaili, S., Baghban, A. A., & Jaberzadeh, S. (2016). Measurement of superficial and deep abdominal muscle thickness: An ultrasonography study. *Journal of Physiological Anthropology*, *35*(1), 1–5. https://doi.org/10.1186/S40101-016-0106-6/TABLES/4

Tanaka, Y., Nakashima, A., Feng, H., Mizuno, K., Yamada, M., Yamada, Y., Yokoyama, Y., & Jinzaki, M. (2021). Analysis of Lap Belt Fit to Human Subjects using CT Images. *Stapp Car Crash Journal*, *65*, 49–90. https://doi.org/10.4271/2021-22-0004

Uriot, J., Potier, P., Baudrit, P., Trosseille, X., Petit, P., Richard, O., Compigne, S., Masuda, M., & Douard, R. (2015a). Reference PMHS Sled Tests to Assess Submarining. *Stapp Car Crash Journal*, *59*, 203–223.

Uriot, J., Potier, P., Baudrit, P., Trosseille, X., Richard, O., & Douard, R. (2015b). Comparison of HII, HIII and THOR dummy responses with respect to PMHS sled tests. *IRCOBI Conference*.

Wang, X., Savonnet, L., Capbern, L., & Duprey, S. (2021). A Case Study on the Effects of Foam and Seat Pan Inclination on the Deformation of Seated Buttocks Using MRI. *IISE*

Transactions on Occupational Ergonomics and Human Factors, *9*(1), 23–32. https://doi.org/10.1080/24725838.2021.1984340/FORMAT/EPUB

Zhai, X., Nauman, E. A., Nie, Y., Liao, H., Lycke, R. J., & Chen, W. W. (2019). Mechanical response of human muscle at intermediate strain rates. *Journal of Biomechanical Engineering*, *141*(4). https://doi.org/10.1115/1.4042900/443642